

High Rayleigh number thermal convection in volumetrically heated spherical shells

Frédéric Deschamps,¹ Chloé Yao,^{2,3} Paul J. Tackley,² and C. Sanchez-Valle³

Received 28 March 2012; revised 31 July 2012; accepted 1 August 2012; published 25 September 2012.

[1] We conducted experiments of isoviscous thermal convection in homogeneous, volumetrically heated spherical shells with various combinations of curvature, rate of internal heating, and Rayleigh number. We define a characteristic temperature adapted to volumetrically heated shells, for which the appropriate Rayleigh number, measuring the vigor of convection, is $Ra_{VH} = \frac{(1+f+f^2)}{3} \frac{\alpha \rho^2 g H D^5}{\eta k \kappa}$, where f is the ratio between the inner and outer radii of the shell. Our experiments show that the scenario proposed by Parmentier and Sotin (2000) to describe convection in volumetrically heated 3D-Cartesian boxes fully applies in spherical geometry, regardless of the shell curvature. The dynamics of the thermal boundary layer are controlled by both newly generated instabilities and surviving cold plumes initiated by previous instabilities. The characteristic time for the growth of instabilities in the thermal boundary layer scales as $Ra_{VH}^{-1/2}$, regardless of the shell curvature. We derive parameterizations for the average temperature of the shell and for the temperature jump across the thermal boundary layer, and find that these quantities are again independent of the shell curvature and vary as $Ra_{VH}^{-0.238}$ and $Ra_{VH}^{-1/4}$, respectively. These findings appear to be valid down to relatively low values of the Rayleigh-Roberts number, around 10^5 .

Citation: Deschamps, F., C. Yao, P. J. Tackley, and C. Sanchez-Valle (2012), High Rayleigh number thermal convection in volumetrically heated spherical shells, *J. Geophys. Res.*, 117, E09006, doi:10.1029/2012JE004090.

1. Introduction

[2] Due to their rheological and physical properties, cores and overlying shells (e.g., silicate mantles or ice layers) of rocky planets and icy moons are or have been animated by convection. The details of the flow pattern, heat transfer, and thermal structure, which in turn influence the evolution of the planetary interiors, depend on several parameters, including the rheology of the material, the presence of phase transitions, and the mode of heating. In addition, intrinsic magnetic fields, if present, and rotation are essential to properly describe the dynamics of an electrically conducting fluid layer, a case that we will not consider here. External and intermediate shells are cooled at their surface, heated at their bottom, and may furthermore include internal heat sources, for instance induced by the decay of radiogenic elements or by tidal dissipation. Planetary cores are also cooled at their top (unless the overlying mantle is unable to extract heat from

them) and may include internal sources of heat (from radiogenic heating), i.e., they are heated only from within.

[3] In a fluid heated from below, two thermal boundary layers (TBL) are present, one at the bottom and the other below the surface. Hot plumes and cold downwellings are generated from the bottom and top TBLs, respectively. Internal sources of heat modify the relative stability of these TBLs. As the amount of internal heating increases, hot plumes are less vigorous, and the flow is progressively controlled by cold downwellings [Travis and Olson, 1994; Sotin and Labrosse, 1999; McNamara and Zhong, 2005; Deschamps et al., 2010; O'Farrell and Lowman, 2010]. An important consequence is that less heat may be extracted from the underlying layer. In contrast, in a volumetrically heated fluid, only one TBL is present, below the surface. The flow is fully driven by cold downwellings, and return flow brings material back to the surface.

[4] Howard [1966] described high Rayleigh number thermal convection with a scenario based on the conductive thickening of TBLs. Below the surface of a fluid that is cooled from the top, a TBL grows by conduction until it reaches a critical thickness and becomes unstable. The instability rapidly sinks downward, forming a cold blob (or downwelling), and a new TBL starts to develop again. A symmetric scenario describes the growth of hot instabilities in a layer heated from the bottom. Based on their numerical experiments, Parmentier and Sotin [2000] showed that Howard's scenario describes very well thermal convection in

¹Institute of Earth Sciences, Academia Sinica, Taipei, Taiwan.

²Institute of Geophysics, Swiss Federal Institute of Technology Zurich, Zurich, Switzerland.

³Institute of Geochemistry and Petrology, Swiss Federal Institute of Technology Zurich, Zurich, Switzerland.

Corresponding author: F. Deschamps, Institute of Earth Sciences, Academia Sinica, 128 Academia Rd., Sec. 2, Nangang, Taipei 11529, Taiwan. (frederic@earth.sinica.edu.tw)

volumetrically heated 3D-Cartesian boxes, but also pointed out some important differences. In particular, they observed that the cold plumes generated by TBL instabilities survive for relatively long periods, and participate in the heat transfer together with the new instabilities. Plumes are finally removed by merging with another at a rate that is balanced by the development of new instabilities.

[5] In this study, we performed a series of numerical experiments of isoviscous thermal convection in volumetrically heated spherical shells, which we analyze following the method developed in *Parmentier and Sotin* [2000]. Our results indicate that the description of thermal convection proposed by *Howard* [1966] and modified by *Parmentier and Sotin* [2000] is also valid in volumetrically heated spherical shells, regardless of the core's size. Furthermore, when using an appropriate temperature scale, the properties of the TBL can be described with parameterizations that are independent of the geometry.

2. Physical Model

[6] To model the convective flow and heat transfer in spherical shells, we solve the conservation equations of mass, momentum, and energy for an incompressible, homogeneous, infinite Prandtl number fluid. We use the shell thickness D as the characteristic length of the system. A useful geometric parameter is the ratio f of the core radius to the total radius of the sphere,

$$f = \frac{R_c}{R_c + D} = \frac{r_c}{r_c + 1}, \quad (1)$$

where R_c and r_c are the dimensional and non-dimensional core radius, respectively. The curvature of the shell is inversely proportional to the parameter f , which varies between 0 for a sphere with no core, and 1 for an infinite slab (3D-Cartesian geometry). The top boundary is isothermal and the bottom heat flux is set to zero, i.e., the fluid is cooled from the top and heated within only. Heating is homogeneous, with an internal heating rate per unit mass H .

[7] In the case of a volumetrically heated fluid, the bottom temperature is not a priori prescribed, and the superadiabatic temperature difference across the shell cannot be used as characteristic temperature scale, as is usually done in Rayleigh-Bénard convection. Instead, temperature may be scaled from the surface conductive temperature gradient. For a spherical shell heated from within, this gradient is [e.g., *Schubert et al.*, 2001]

$$\left. \frac{dT}{dr} \right|_{r=R} = -\frac{\rho HR}{3k} \left(1 - \frac{R_c^3}{R^3} \right), \quad (2)$$

where ρ and k are the density and thermal conductivity of the fluid, and $R = (R_c + D)$ is the total radius of the shell. Noting that $R = D/(1 - f)$, and using the definition of f (equation (1)), the conductive gradient may be written

$$\left. \frac{dT}{dr} \right|_{r=R} = -\frac{(1+f+f^2)}{3} \frac{\rho HD}{k}. \quad (3)$$

With D as length scale, the characteristic surface conductive temperature gradient is $\Delta T/D$, where ΔT is an implicit characteristic temperature difference associated with the

conducting state. Setting the non-dimensional value of this gradient to one, the non-dimensionalization of equation (3) defines the temperature scale as

$$\Delta T = \frac{(1+f+f^2)}{3} \frac{\rho HD^2}{k}. \quad (4)$$

An important observable is the average surface heat flux, Φ_{surf} . For a spherical shell heated from within only, this flux can be written

$$\Phi_{\text{surf}} = \frac{(1+f+f^2)}{3} \rho HD, \quad (5)$$

where the geometric factor $a = (1+f+f^2)/3$ is imposed by the conservation of energy. Given the temperature scale defined in equation (4), Φ_{surf} is the characteristic heat flux, so that the observed non-dimensional surface heat flux, $\vartheta_{\text{surf}} = \Phi_{\text{surf}} D / k \Delta T$, should be equal to 1.

[8] With equation (4) as characteristic temperature difference and D^2/κ as characteristic time, where κ is the thermal diffusivity, the system of non-dimensional conservation equations we solve is

$$\begin{cases} \nabla^2 \mathbf{u} - \nabla P = -Ra_{\text{vH}} T_{\text{vH}} \mathbf{e}_z \\ \nabla \cdot \mathbf{u} = 0 \\ \frac{\partial T_{\text{vH}}}{\partial t} = \nabla \cdot \nabla T_{\text{vH}} - \mathbf{u} \cdot \nabla T_{\text{vH}} + h_{\text{vH}} \end{cases}, \quad (6)$$

where \mathbf{u} and P are the non-dimensional velocity and non-hydrostatic pressure. $T_{\text{vH}} = (T - T_{\text{surf}})/\Delta T$ is the non-dimensional temperature, where T_{surf} is the dimensional surface temperature and ΔT is given by equation (4). The appropriate Rayleigh number (controlling the vigor of convection) is the Rayleigh-Roberts number,

$$Ra_{\text{vH}} = \frac{(1+f+f^2)}{3} \frac{\alpha \rho^2 g HD^5}{\eta k \kappa}, \quad (7)$$

where α is the fluid thermal expansivity and g the surface acceleration of gravity, and the non-dimensional rate of internal heating is

$$h_{\text{vH}} = \frac{3}{(1+f+f^2)} \quad (8)$$

and satisfies the conservation of energy with the constraint that the non-dimensional surface heat flux is equal to 1.

[9] Fixing f to 1 in equations (4) to (7), the geometric factor $a = (1+f+f^2)/3$ reduces to 1, and one finds the 3D-Cartesian expressions of the characteristic temperature and Rayleigh-Roberts number for a volumetrically heated fluid. For a sphere, on the other hand, $f = 0$ and the geometric factor is equal to 1/3. Note that taking the outer radius of the shell, $R = R_c + D$, as the characteristic length, *Schubert et al.* [2001] proposed another definition of the Rayleigh number in a volumetrically heated shell. With R_c as the characteristic length, the geometric factor we introduced in equations (4) to (8) changes to $(1 - f^3)/3$. Both definitions are of course equivalent for a sphere ($f = 0$, and $R_c = D$). An advantage of

taking D as the characteristic length is that it allows continuity between the parameterizations in spherical and 3D-Cartesian geometries.

[10] It is useful to keep in mind that the Rayleigh number, and temperatures in the Rayleigh-Bénard (Ra and T) and Rayleigh-Roberts (Ra_{VH} and T_{VH}) descriptions are related by

$$Ra = \frac{3}{(1+f+f^2)} \frac{1}{h} Ra_{\text{VH}}, \quad (9)$$

and

$$T = \frac{(1+f+f^2)}{3} h T_{\text{VH}}, \quad (10)$$

where

$$h = \frac{\rho H D^2}{k \Delta T} \quad (11)$$

is the non-dimensional rate of internal heating in Rayleigh-Bénard description, and ΔT the superadiabatic temperature jump. For practical reasons, in our experiments we prescribe Ra , f , and h . Given f and h , we then adjust the value of Ra to the desired value of Ra_{VH} using equation (9).

[11] Calculations are performed on Yin-Yang staggered grids using STAGYY [Tackley, 2008]. The solver is a Jacobi relaxation method, and the convergence of the momentum and pressure equations is accelerated using a multigrid method [e.g., Stüben and Trottenberg, 1982]. Time stepping in the conservation of energy follows an explicit MPDATA [Smolarkiewicz, 1984] algorithm for advective terms, and a second-order finite difference scheme for diffusive terms. The Yin-Yang grid [Kageyama and Sato, 2004] consists of two strips of equal size that are combined to generate a spherical surface. The strips' geometry induces small overlaps at the strips' boundaries. STAGYY uses the minimum overlap defined by Kageyama and Sato [2004], in which the cells located at the corners of one strip that are entirely contained within the other strip are eliminated. Scalar and vectorial quantities are calculated at the middle and on the sides of each cell, respectively. To better describe the thermal boundary layer below the surface of the fluid, the grid is vertically refined at the top of the domain. Both the surface and the bottom of the shells are free slip. The initial condition for the temperature consists of 3D-random perturbations, and the calculations are carried on until a quasi-equilibrium state is reached. At this stage, the mean temperature and surface heat flux oscillate around constant time-averaged values. For cases with high Rayleigh number, we set the initial condition with a quasi-equilibrium solution obtained for a case with a lower Rayleigh number, which significantly reduces the computational time needed to reach the quasi-equilibrium solution.

3. Numerical Experiments and Results

[12] Using the setup detailed in section 2, we conducted 34 numerical experiments (including 3 experiments in 3D-Cartesian geometry) varying Ra , f , and h such that Ra_{VH} is between 10^5 and 10^{10} (Table 1). Note that the same results maybe be obtained by setting $h = 1$ in all experiments and

varying Ra accordingly. For most cases, we set the grid resolution $n_{\text{phi}} \times n_{\text{theta}} \times n_r$ to $512 \times 512 \times 64$ points, corresponding to Yin and Yang strips with 128×384 points each. For experiments with large ($\geq 3.0 \times 10^7$) Rayleigh-Roberts number, we increased the vertical resolution to 128 points. Together with the radial grid refinement at the top of the shell, this allows a correct sampling of the thermal boundary layer at the top of the system. In addition, for cases combining a large core and a large Rayleigh number (typically, $f \geq 0.6$ and $Ra_{\text{VH}} \geq 10^8$), we extended the horizontal resolution of the Yin and Yang strips to 192×576 points to have enough lateral resolution. For 3D-Cartesian cases, we assumed reflecting sidewalls, we fixed the horizontal to vertical aspect ratio to 4, and we set the resolution to $256 \times 256 \times 128$ or $384 \times 384 \times 192$, depending on the value of Ra_{VH} .

[13] In a fluid heated from within and cooled on the top, a thermal boundary layer (TBL) develops below the surface, but not at the bottom of the fluid. As a consequence, the horizontally averaged temperature first increases with depth up to a maximum value and then slowly decreases throughout the rest of the domain (Figure 1). Setting the surface non-dimensional temperature to zero, the maximum in the horizontally averaged temperature profile, T_{max} , is a measure of the temperature jump across the TBL, δT_{TBL} . The characteristic temperature and heat flux we use further imply that the non-dimensional thickness of the TBL, δ_{TBL} , is numerically equal to δT_{TBL} . Table 1 lists the volumetrically averaged temperature, $\langle T_{\text{VH}} \rangle$, temperature jump across the TBL, δT_{TBL} , and the horizontally averaged temperature at the bottom of the shell, T_{bot} . All temperatures listed in Table 1 are scaled with equation (4), and time-averaged over a few (usually between 10 and 20) pseudo-periods after the quasi-equilibrium is reached. Figure 2 shows slices of snapshots of the non-dimensional temperature for selected cases. Snapshots are taken during the quasi-equilibrium stage. Again, in all plots the temperature is scaled with equation (4). Finally, in all our experiments we checked that the horizontally and time-averaged non-dimensional surface heat flux is equal to 1 with great accuracy (1% and less), as one would expect when quasi-equilibrium is reached.

[14] A careful examination of Table 1, and Figures 1 and 2 indicates that the average temperature, $\langle T_{\text{VH}} \rangle$, decreases with increasing Rayleigh number, Ra_{VH} , but does not depend on core size, measured with f . For instance, the cases shown in Figures 2a and 2b, which have different core size and close values of Ra_{VH} ($f = 0.20$ and $Ra_{\text{VH}} = 3.0 \times 10^6$, vs $f = 0.55$ and $Ra_{\text{VH}} = 3.5 \times 10^6$), have average properties (Table 1) that are close to one another. Like $\langle T_{\text{VH}} \rangle$, the temperature jump across the TBL decreases with increasing Ra_{VH} , as indicated by Table 1 and Figure 1. Interestingly, the values of $\langle T_{\text{VH}} \rangle$ and δT_{TBL} we measured, including those for the 3D-Cartesian cases, fit well along power laws of Ra_{VH} (Figure 3). Least squares fits of our data lead to

$$\langle T_{\text{VH}} \rangle = \frac{1.744}{Ra_{\text{VH}}^{0.238}} \quad (12)$$

and

$$\delta T_{\text{TBL}} = \frac{2.508}{Ra_{\text{VH}}^{0.251}}. \quad (13)$$

Table 1. Numerical Experiments of Convection in Volumetrically Heated Spherical Shells^a

f	Ra_{VH}	h	Resolution	$\langle T_{\text{VH}} \rangle$	δT_{TBL}	T_{bot}	$P (\times 10^{-2})$
0.20	2.98×10^6	20.0	$128 \times 384 \times 64$	0.04958	0.06016	0.04710	0.7542
-	1.49×10^8	40.0	$128 \times 384 \times 128$	0.01967	0.02246	0.01689	0.0964
-	5.02×10^9	45.0	$128 \times 384 \times 128$	0.00841	0.00918	0.00722	0.0177
0.30	1.18×10^6	15.0	$128 \times 384 \times 128$	0.06133	0.07545	0.05866	1.4876
-	3.24×10^7	25.0	$128 \times 384 \times 128$	0.02836	0.03280	0.02449	0.2521
-	2.04×10^8	40.0	$128 \times 384 \times 128$	0.01827	0.02069	0.01539	0.0903
0.40	5.20×10^5	10.0	$128 \times 384 \times 64$	0.07438	0.09239	0.06763	1.6660
-	1.66×10^6	3.2	$128 \times 384 \times 64$	0.05713	0.06897	0.05246	1.0442
-	5.20×10^6	10.0	$128 \times 384 \times 64$	0.04392	0.05194	0.03921	0.5797
-	1.66×10^7	32.0	$128 \times 384 \times 64$	0.03337	0.03879	0.02900	0.3329
-	2.03×10^9	30.0	$128 \times 384 \times 128$	0.01050	0.01147	0.00882	0.0331
0.55	1.98×10^5	1.0	$128 \times 384 \times 64$	0.09465	0.11798	0.08392	3.1047
-	3.09×10^5	5.0	$128 \times 384 \times 64$	0.08479	0.10455	0.07517	2.8153
-	6.18×10^5	10.0	$128 \times 384 \times 64$	0.07229	0.08775	0.06422	1.6952
-	1.98×10^6	3.2	$128 \times 384 \times 64$	0.05531	0.06568	0.04866	0.9008
-	3.46×10^6	5.6	$128 \times 384 \times 64$	0.04850	0.05709	0.04227	0.7502
-	6.18×10^6	10.0	$128 \times 384 \times 64$	0.04232	0.04943	0.03641	0.5018
-	1.98×10^7	32.0	$128 \times 384 \times 64$	0.03215	0.03704	0.02679	0.3080
-	6.18×10^7	10.0	$128 \times 384 \times 128$	0.02447	0.02781	0.01999	0.1539
0.60	7.84×10^7	50.0	$128 \times 384 \times 128$	0.02308	0.02610	0.01870	0.1274
-	3.40×10^8	40.0	$192 \times 576 \times 128$	0.01617	0.01799	0.01340	0.0650
0.70	3.65×10^5	5.0	$128 \times 384 \times 64$	0.08253	0.09972	0.07184	2.5703
-	7.30×10^5	10.0	$128 \times 384 \times 64$	0.07002	0.08339	0.06114	1.7776
-	2.34×10^6	3.2	$128 \times 384 \times 64$	0.05343	0.06256	0.04584	1.0356
-	7.30×10^6	10.0	$128 \times 384 \times 64$	0.04092	0.04723	0.03424	0.4760
-	2.34×10^7	32.0	$128 \times 384 \times 64$	0.03104	0.03534	0.02552	0.2757
-	5.11×10^8	50.0	$192 \times 576 \times 128$	0.01468	0.01612	0.01202	0.0499
0.80	3.17×10^5	30.0	$128 \times 384 \times 64$	0.08586	0.10301	0.07456	2.6452
-	9.76×10^5	40.0	$128 \times 384 \times 64$	0.06586	0.07743	0.05673	1.3680
-	1.20×10^7	40.0	$128 \times 384 \times 128$	0.03641	0.04136	0.03013	0.3693
-	4.55×10^7	35.0	$192 \times 576 \times 128$	0.02643	0.02963	0.02180	0.1995
1.00	10^7	10.0	$256 \times 256 \times 128$	0.03811	0.04317	0.03156	0.4076
-	10^8	10.0	$256 \times 256 \times 128$	0.02175	0.02424	0.01750	0.1358
-	10^9	10.0	$384 \times 384 \times 192$	0.01249	0.01369	0.00987	0.0366

^aInput parameters are the ratio f between the inner and outer radii of the shell ($f = 1.0$ indicates 3D-Cartesian geometry), the Rayleigh-Roberts number Ra_{VH} , which is given by equation (7) and can be related to the Rayleigh-Bénard number through equation (9), and the non-dimensional rate of internal heating (in Rayleigh-Bénard description) h , given by equation (11). Output observables are the non-dimensional temperature of the well-mixed interior, $\langle T_{\text{VH}} \rangle$, the temperature jump across the thermal boundary layer, δT_{TBL} , the horizontally averaged temperature at the bottom of the shell T_{bot} , and the period P of heat flux oscillations. All temperatures are scaled with equation (4) and time-averaged over several periods after a quasi-equilibrium is reached. For spherical cases ($f < 1.0$), the resolution, $n_{\text{phi}} \times n_{\text{theta}} \times n_r$, indicates the size of the Yin volumes, the corresponding Yang volumes having $n_{\text{theta}} \times n_{\text{phi}} \times n_r$ points.

Equation (13) further fits the numerical experiments of *Parmentier and Sotin* [2000] performed in 3D-Cartesian boxes with aspect ratio of 1 or 2. Note that their best fit multiplicative constant and exponent (respectively 2.2312 and -0.2448) are slightly different from ours. Equation (13) is consistent with thermal boundary layer analysis, which predicts that the temperature jump in the TBL scales as $Ra_{\text{VH}}^{-1/4}$ (section 4). To complete the description of the horizontally averaged thermal structure, we derived a parameterization for the horizontally averaged bottom temperature T_{bot} , which is not known a priori but may have planetary applications. Again, T_{bot} fit well along a power law of Ra_{VH} (Figure 3, bottom series of points),

$$T_{\text{bot}} = \frac{1.755}{Ra_{\text{VH}}^{0.248}}. \quad (14)$$

Our results indicate that, in a volumetrically heated fluid, the characteristic properties of the temperature distributions, and in particular the average temperature of the fluid and the temperature jump across the TBL, are quantified with simple parameterized laws of the Rayleigh-Roberts number, independent of the amount of internal heating and of the geometry. The influences of the geometry and of the amount of

internal heating are implicitly included in the definitions of the temperature scale (equation (4)) and therefore of the Rayleigh number (equation (7)). It should be noted that, as detailed in section 2, the choice of the temperature scale is not ad hoc, but is imposed by the properties of the system (here, the geometry and the mode of heating). Equation (4) is therefore well suited to describe volumetrically heated shells.

[15] Figure 3 suggests that the parameterizations (12) and (13) still explain the observed $\langle T_{\text{VH}} \rangle$ and δT_{TBL} for cases with relatively low Rayleigh number, down to about 10^5 . This value is much larger than the critical Rayleigh number for the onset of instability in volumetrically heated shells. Using linear stability analysis, *Zebib et al.* [1983] found that this number decreases with increasing core radius. Note that the Rayleigh number defined in *Zebib et al.* [1983] is similar to that in equation (7), except that it does not include the geometric factor $(1 + f + f^2)/3$. Using the definition in equation (7), the critical Rayleigh number calculated by *Zebib et al.* [1983] ranges from 3091 for $f = 0$ to 1023 for $f = 0.7$. We did additional experiments with $Ra_{\text{VH}} < 10^5$, and found that the values of $\langle T_{\text{VH}} \rangle$ and δT_{TBL} do not fit along equations (12) and (13) below a value of Ra_{VH} around 5.0×10^4 , suggesting the existence of an intermediate regime between the onset of

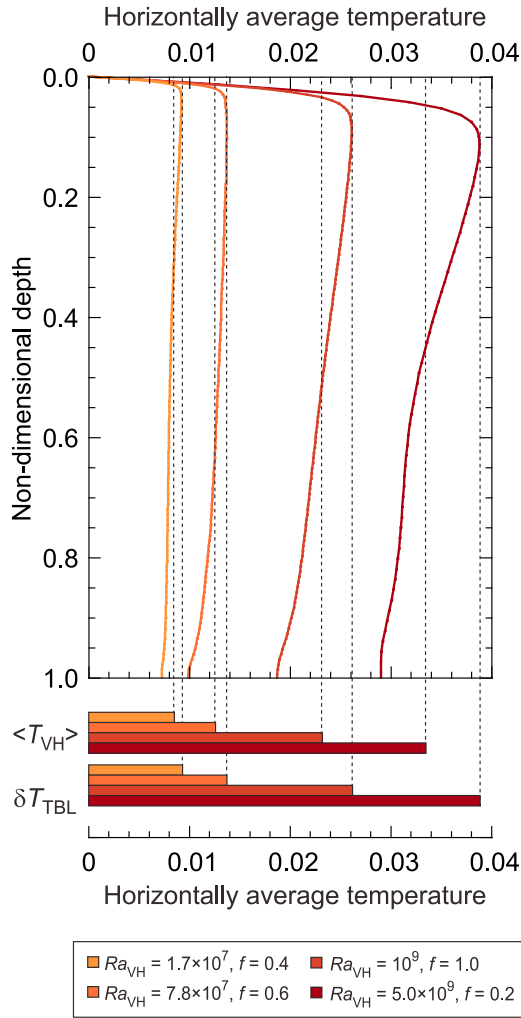


Figure 1. Time and horizontally averaged temperature profiles obtained for various Rayleigh number (Ra_{VH}) and core size, measured by the ratio f between inner and outer radii of the shell ($f = 1$ indicates 3D-Cartesian geometry). From right to left: $Ra_{VH} = 1.7 \times 10^7$ and $f = 0.4$, $Ra_{VH} = 7.8 \times 10^7$ and $f = 0.6$, $Ra_{VH} = 10^9$ and $f = 1.0$, and $Ra_{VH} = 5.0 \times 10^9$ and $f = 0.2$. The horizontal bars below the profiles represent the temperature jump in the TBL (bottom series of bars) and the volumetrically averaged temperature (top series of bars) for each case.

convection, and the regime described in this study. Interestingly, in the case of a bottom heated fluid, thermal boundary layer theory also does not work at low Rayleigh number.

4. Dynamics of the Thermal Boundary Layer

[16] A central point in the description of high Rayleigh number thermal convection proposed by *Howard* [1966] is that the TBL thickens by conduction until it reaches a critical thickness. When this limit is reached, the TBL becomes unstable, i.e., a cold plume is generated and quickly sinks to the bottom of the fluid. A conductive temperature distribution is then restored in the region where the instability occurred, allowing a new TBL to grow again. The numerical experiments of *Parmentier and Sotin* [2000] globally

validated this scenario, but also pointed out that cold plumes are maintained during longer periods of time than suggested by *Howard* [1966]. Furthermore, they showed that when quasi-equilibrium is reached the creation of new instabilities is balanced by the coalescence of existing plumes, leaving the average plumes density constant in time. Figure 4, which plots a time sequence of the temperature distribution for a case with $f = 0.40$, shows that both new instabilities and persisting cold plumes are simultaneously present at different locations. The growth of instabilities can be seen on isosurfaces (Figure 4, left), where new holes are opening, and in the top section of polar slices (Figure 4, right). We also observe plume coalescence, as seen for instance in the region around 50° latitude and 250° longitude (maps in Figure 4, middle). Figure 4 further indicates that cold plumes eventually die by detaching from the TBL, as in the bottom right section of polar slices. It is interesting to note that the number of plumes present per unit surface does not vary in time. In the section represented on maps (covering $1/6$ of the total surface), 6–7 plumes are present during the entire sequence (the total number of plumes over the entire surface, not shown here, varying between 34 and 36). These observations suggest that the modified scenario proposed by *Parmentier and Sotin* [2000] also happens in spherical geometry.

[17] First, it is worth noting that the temperature jump across the TBL is fully consistent with thermal boundary layer analysis. At the bottom of the TBL the radial conductive and advective heat flux balance

$$k \frac{\Delta T_{TBL}}{d_{TBL}} = \rho C_p u_z T_{TBL}, \quad (15)$$

where ΔT_{TBL} is the dimensional temperature jump across the TBL, d_{TBL} its dimensional thickness, T_{TBL} and u_z the dimensional temperature and radial component of the velocity at the bottom of the TBL, and C_p the heat capacity of the fluid. The viscous and buoyancy forces are also balancing at the bottom of the TBL (as everywhere else in the fluid),

$$\alpha \rho g \Delta T_{TBL} = \eta \frac{u_z}{d_{TBL}^2}. \quad (16)$$

Combining equations (15) and (16), and assuming that T_{TBL} scales as ΔT_{TBL} , and that the horizontally averaged heat flux across the TBL, Φ_{TBL} , does not depend on depth and is equal to $k \Delta T_{TBL} / d_{TBL}$, one gets

$$\Delta T_{TBL}^4 \sim \frac{\eta \kappa \Phi_{TBL}^3}{\alpha g \rho k^3}. \quad (17)$$

Because Φ_{TBL} is assumed constant throughout the TBL, it is equal to the surface heat flux given in equation (5). Taking D as length scale and equation (4) as temperature scale, the non-dimensional temperature jump across the TBL satisfies

$$\delta T_{TBL} \sim \left[\frac{3}{(1+f+f^2)} \frac{\eta \kappa}{\alpha \rho^2 g H D^5} \right]^{1/4} = Ra_{VH}^{-1/4}. \quad (18)$$

Following *Parmentier and Sotin* [2000], we have then compared the horizontally and time-averaged profiles of the non-

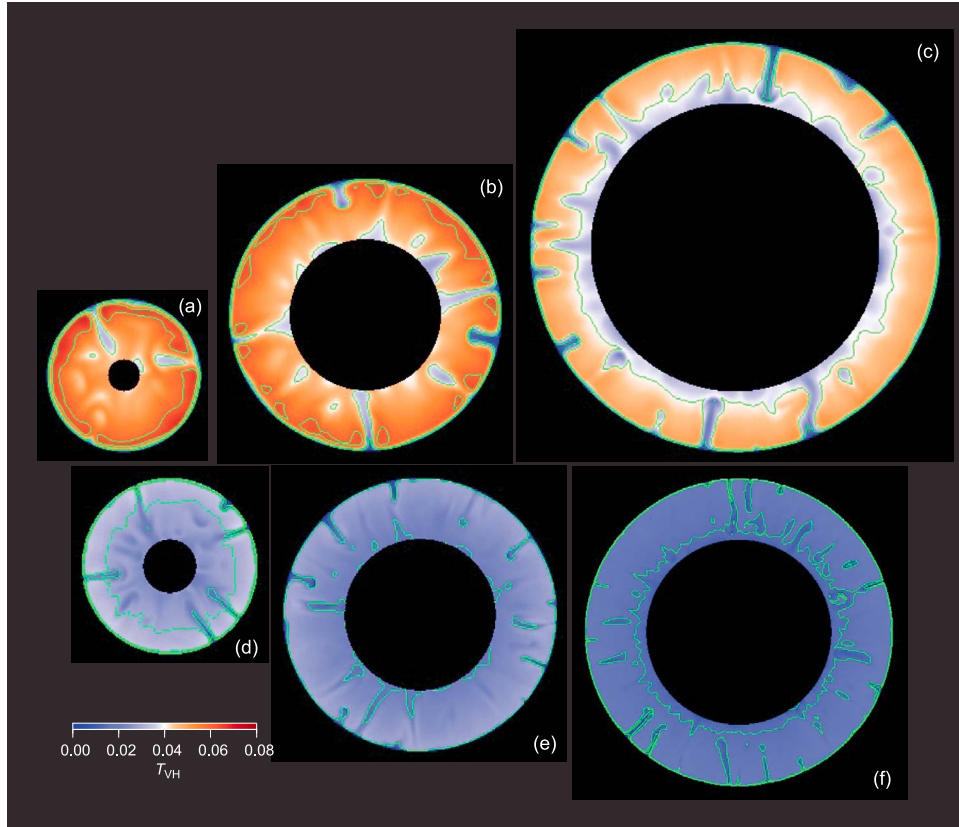


Figure 2. Slices of the non-dimensional temperature (scaled with equation (4)) for 6 cases with various core size. Panels are scaled such that thickness of the shell is the same in all panels. Snapshots are taken during the quasi-equilibrium stage. The Rayleigh number Ra_{VH} , given by equation (7), increases from Figures 2a to 2f. (a) $f = 0.20$ and $Ra_{VH} = 3.0 \times 10^6$. (b) $f = 0.55$ and $Ra_{VH} = 3.5 \times 10^6$. (c) $f = 0.70$ and $Ra_{VH} = 7.3 \times 10^6$. (d) $f = 0.30$ and $Ra_{VH} = 3.2 \times 10^2$. (e) $f = 0.55$ and $Ra_{VH} = 6.2 \times 10^7$. (f) $f = 0.60$ and $Ra_{VH} = 3.4 \times 10^8$.

dimensional temperature observed in our experiments, with the expression given by Howard [1966],

$$T_{VH}(\xi) = \delta T_{TBL} \left[1 - (1 + 2\xi^2) \operatorname{erfc}(\xi) + \frac{2}{\sqrt{\pi}} \xi e^{-\xi^2} \right] \quad (19)$$

where

$$\xi = \frac{z}{2\sqrt{\pi t_c}}, \quad (20)$$

z is the non-dimensional depth, and t_c is the non-dimensional time (scaled with D^2/κ) for the growth of instabilities in the TBL. Noting that when quasi-equilibrium is reached the time-averaged conductive heat flux, given by the solution to half-space cooling $2k\Delta T/\sqrt{\pi\kappa t}$, and the observed heat flux, here given by equation (5), should be equal, an expression for t_c is [Parmentier and Sotin, 2000]

$$t_c = \frac{4}{\pi} \delta T_{TBL}^2, \quad (21)$$

where we again use equation (4) to scale the temperature jump in the TBL. We calculated t_c either by using equation (21) and the values of δT_{TBL} in Table 1, or by searching for the value of t_c that provides the best least squares fit of equation (19) to the observed profiles of temperature, and found that t_c varies as $Ra_{VH}^{-1/2}$ for both these two methods (Figure 5, bottom and

middle series of points). Equation (19) explains the time and horizontally averaged profiles from our experiments very well, with least squares fit around 99% whatever the case. The values of t_c calculated with equation (21) are however larger by 60% on average than those obtained by the best fit of equation (19), a result that may be due to the fact that both existing cold plumes and new instabilities contribute to remove the TBL [Parmentier and Sotin, 2000].

[18] Another consequence of the persistence of cold plumes is that they participate in the heat transfer [Parmentier and Sotin, 2000]. When quasi-equilibrium is reached, variations in the number and distribution of plumes therefore induce small variations in the surface heat flux around an average value that remains constant in time. If heat flux is scaled with equation (5), this value is equal to one for all cases. In our experiments, oscillations around the time-averaged value have amplitude of a few (up to 4) percent. We do not observe a systematic relationship between the amplitude of these oscillations and the Rayleigh number. In contrast, when time is scaled with the characteristic diffusion time across the whole shell (D^2/κ), their periods P clearly decrease with increasing Rayleigh number (Figure 6, left column). We measured P by counting the number of oscillations within a time window containing 10 or more oscillations, and found that it scales roughly as $Ra_{VH}^{-1/2}$ (right column in Table 1, and top series of points in Figure 5). Rescaling the time with the characteristic

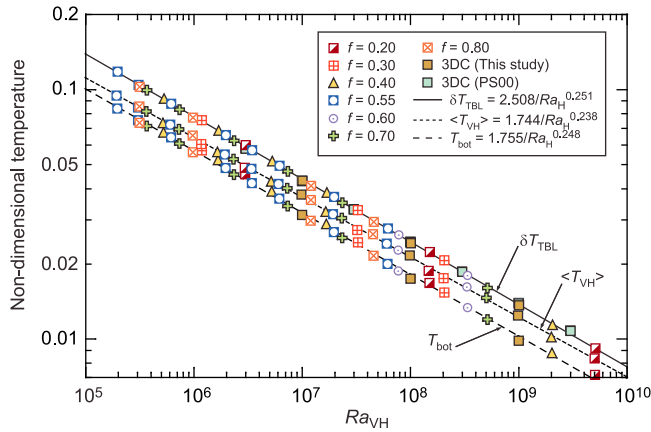


Figure 3. Volumetrically averaged temperature ($\langle T_{VH} \rangle$, middle series of points), temperature jump across the thermal boundary layer (δT_{TBL} , top series of points), and horizontally averaged temperature at the bottom of the shell (T_{top} , bottom series of points) as a function of the Rayleigh number. All temperatures are time-averaged and scaled with equation (4). Experiments with various core size are denoted with different symbols (see legend). The black dotted, plain, and dashed lines show the scaling providing the best fit to the data, and are given by equations (12), (13), and (14), respectively. Also represented are the temperature jump across the TBL for the 3D-Cartesian experiments of *Parmentier and Sotin* [2000] (light blue squares).

time for the growth of instabilities in the TBL (equation (21)), the period of the oscillations is independent of the Rayleigh number, and is roughly equal to $t_c/2$.

5. Comparison With Mixed Heated Spherical Shells

[19] The observation that the dynamics of a TBL in volumetrically heated systems does not depend on the geometry of the system contrasts with results obtained for bottom and mixed heated fluids [*Deschamps et al.*, 2010]. In these cases, two TBLs are present, at the top and at the bottom of the fluid, respectively. For an isoviscous, 3D-Cartesian system heated from below, these two layers are geometrically and dynamically symmetric. Both spherical geometry and internal heating break this symmetry, and have strong influence on the properties of the top and bottom TBLs, resulting in parameterizations for average temperature and heat flux that explicitly depend on h and f [*Sotin and Labrosse*, 1999; *Moore*, 2008; *Shahnas et al.*, 2008, *Deschamps et al.*, 2010]. Even when rescaled with equation (4), the average temperatures observed in these studies do not fit along a power law of the Rayleigh-Roberts number and still have a strong dependence on h and f .

[20] Based on the results discussed in section 3, a new parameterization for the average temperature in a mixed heating fluid may be attempted. This expression should satisfy two boundary conditions, corresponding to the average temperatures for pure bottom and volumetric heating, respectively. For pure bottom heating the average temperature, $\langle T_{BH} \rangle$, depends only on the shell curvature through the parameter f and goes to zero for $f = 0$ [*Vangelov and Jarvis*,

1994; *Jarvis et al.*, 1995; *Shahnas et al.*, 2008; *Deschamps et al.*, 2010]. Here, we will assume that $\langle T_{BH} \rangle$ follows the law suggested by *Deschamps et al.* [2010], $f^2/(1+f^2)$. Note that $\langle T_{BH} \rangle = 0$ for $f = 0$, which corresponds to pure internal heating. The second end-member is obtained by rescaling the average temperature for pure internal heating with the super-adiabatic temperature jump. For this, we replace Ra_{VH} and $\langle T_{VH} \rangle$ in equation (12) by their expressions in equations (9) and (10), which introduces *de facto* a dependence on f . The average temperature in a mixed heated fluid should therefore follow

$$\langle T \rangle = \frac{f^2}{1+f^2} + C \left[\frac{(1+f+f^2)}{3} \right]^{0.762} \frac{h^{0.762}}{Ra^{0.238}}, \quad (22)$$

where C is a parameter that depends on f . This additional dependency is needed to explain the data from numerical experiments with mixed heating [*Shahnas et al.*, 2008; *Deschamps et al.*, 2010], and may be related to the fact that the relative size of the top and bottom TBL strongly varies with f . With decreasing f , the average temperature tends to that for pure internal heating, i.e., it is dominated by the second term of the right-hand-side in equation (22). Following *Deschamps et al.* [2010], we assumed that C depends linearly on f , $C = (c_1 + c_2 f)$, where c_1 and c_2 are two constants. Ideally, to match the scaling obtained for pure internal heating (equation (12)), c_1 should be equal to 1.744. We inverted the results of *Deschamps et al.* [2010], consisting of 56 experiments with mixed heating, for values of c_1 and c_2 using a generalized nonlinear inversion method [*Tarantola and Valette*, 1982], and found $c_1 = 1.84 \pm 0.02$ and $c_2 = -0.85 \pm 0.04$, with a χ^2 equal to 68, indicating that the result of the inversion is very good. Fixing c_1 to 1.744 and inverting for c_2 only, we found $c_2 = -0.70 \pm 0.01$ with a χ^2 equal to 81, still indicating that the result of the inversion is good. We therefore suggest the following parameterization to describe the average temperature in spherical shells heated from below and/or from within,

$$\langle T \rangle = \frac{f^2}{1+f^2} + (1.744 - 0.70f) \left[\frac{(1+f+f^2)}{3} \right]^{0.762} \frac{h^{0.762}}{Ra^{0.238}}. \quad (23)$$

Figure 7a indicates that the average temperature observed in various experiments, including those from *Sotin and Labrosse* [1999], *O'Farrell and Lowman* [2010], *Shahnas et al.* [2008], and *Deschamps et al.* [2010] are very well explained by equation (23). Interestingly, the experiments of *O'Farrell and Lowman* [2010] with negative values of h , modeling the cooling of the system, are well explained by equation (23) provided that h is replaced by its absolute value, and C by its opposite value, i.e., $-(1.744 - 0.70f)$. It is also interesting to note that *O'Farrell and Lowman* [2010] did calculations in 3D-Cartesian geometry with different aspect ratios, and found that the average temperature does not vary with aspect ratio. In Figure 7a, we also represented the temperature at mid-depth observed in the 2D-Cartesian numerical experiments of *Moore* [2008], which include cases with very high rate of internal heating (up to $h = 100$). Note that the temperature at mid-depth defined by *Moore* [2008] is numerically close to but slightly different from

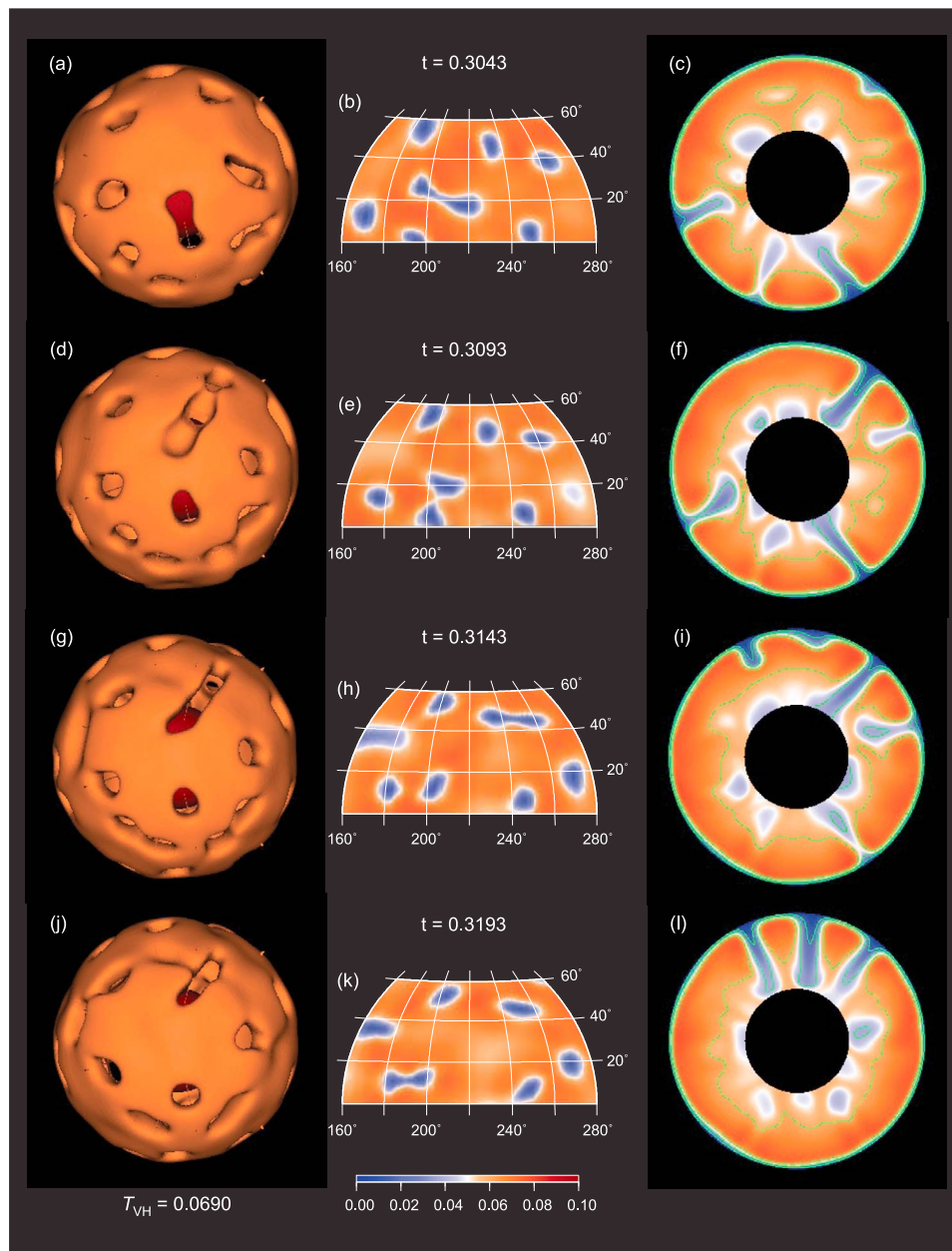


Figure 4. A time-sequence of the temperature evolution for the case $Ra_{\text{VH}} = 1.7 \times 10^6$ and $f = 0.40$. (left) Isosurfaces of the non-dimensional temperature (scaled with equation (4)) for $T_{\text{VH}} = 0.06897$, corresponding to the bottom of the thermal boundary. (middle) Maps of the temperature distribution below the TBL in a region extending from 10° to 60° in latitude, and from 160° to 280° in longitude. (right) Polar slices of the temperature distribution. The sequence was taken during the quasi-equilibrium stage, and its duration is approximately equal to the period of the heat flux oscillations measured for this case.

the volume average temperature. Equation (23) fits well most of *Moore* [2008] experiments, but clearly fails to explain those with average temperature larger than about 1.3. A possible explanation for this disagreement is a fundamental change in the mechanism controlling instabilities in the TBL [Moore, 2008]. In bottom heated and mixed heated fluids, these instabilities are controlled by both TBL thickening and interactions with the plumes that originate from the opposite TBL. These interactions prevent thermal boundary

layer analysis to provide a fine description of the TBL properties (and in particular of the temperature jump across the TBL, see below). The volumetrically averaged temperature, by contrast, is still well described by parameterization such as equation (23) as long as the heat flux at the bottom is positive (in which case a TBL, although small, is present). However, when the rate of internal heating is larger than a critical value h_c , heat cannot be entirely transported toward the surface. The fluid is cooled both at its top and at its bottom, i.e., the heat flux

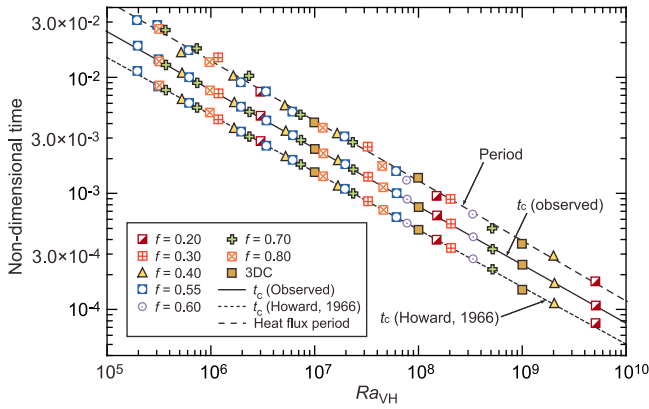


Figure 5. Characteristic conductive time t_c for the growth of instability in the thermal boundary layer as a function of the Rayleigh-Roberts number, and calculated either from surface heat flux balance (equation (21), middle series of points) or least square fit to Howard [1966] formulation (equation (19), bottom series of points). The measured period of the oscillations in the surface heat flux is also shown (P , top series of points). Experiments with various core size are denoted with different symbol (see legend). The black dashed and plain lines shows the scaling providing the best fit to the data.

at the bottom of the fluid is negative. At $h = h_c$, the bottom heat flux is equal to zero, which is equivalent to a purely volumetrically heated system. It is important to note that the value of h_c increases with increasing Ra , since larger Ra promotes heat transport toward the surface.

[21] The validity of equation (23) may thus be restricted to certain ranges of h and Ra , i.e., it may not describe the average temperature of the system if this temperature is larger than an upper limit T_c . It is difficult to estimate T_c from Figure 7a. Data from Moore [2008] are well explained up to values of $\langle T \rangle$ around 1.2, but those from Deschamps et al. [2010] are well explained up to $\langle T \rangle$ around 2.0 (although the agreement appears slightly less good for values of $\langle T \rangle$ larger than 1.5). This is of course partly due to the fact that parameters in equation (23) were obtained using the data from Deschamps et al. [2010] only. Furthermore, it cannot be excluded that T_c depends on the geometry. Moore [2008] defines two parameterizations for h_c , which, together with his parameterization for the average temperature, can be used to estimate T_c . His parameterization based on the temperature jump in the bottom TBL predicts $T_c = 1.06$, whereas his parameterization based on the bottom heat flux implies that T_c slightly depends on Ra and varies between 1.18 and 1.02 in the range $10^4 \leq Ra \leq 10^8$. An estimate of T_c may be deduced directly from data, assuming that it is given by the value of $\langle T \rangle$ for which the bottom heat flux becomes negative.

[22] In Figure 7b, we plotted the non-dimensional bottom heat flux Nu_{bot} as a function of $\langle T \rangle$ using data from several studies. When Nu_{bot} was not listed, we calculated it from the non-dimensional surface heat flux Nu_{top} and assumed conservation of energy,

$$Nu_{bot} = Nu_{top}/f^2 - \frac{(1+f+f^2)}{3}h. \quad (24)$$

The data from Moore [2008], Sotin and Labrosse [1999], and Deschamps et al. [2010] suggests that T_c is in the range 1.0–1.1, whatever the geometry. Data from Shahnas et al. [2008] suggest a slightly lower value for T_c . Assuming that $T_c = 1.0$ and is independent of the geometry, we have calculated h_c as a function of the Rayleigh number and for various values of f (Figure 8). Interestingly, for the ranges of Ra and f relevant to planetary shells, typically $f \leq 0.9$ and $10^5 \leq Ra \leq 10^8$, h_c is large, around 10 and more. In the case of the Earth's mantle, for instance, $f = 0.55$ and Ra is between 10^6 and 10^7 , leading to values of h_c in the range 60–100, i.e., much larger than the non-dimensional rate of radiogenic heating in the Earth mantle, around 15. For the outer ice layer of icy moons, $f > 0.8$ and the Rayleigh number may be up to 10^8 , leading again to values of h_c around 100. For comparison, the rate of tidal dissipation within the outer ice layer may be equivalent to about 10^{-10} W/kg [Tobie et al., 2005], leading to values of the non-dimensional volumetric heating around 5. At planetary conditions, equation (23) thus provides a good description of the average temperature in mixed-heated shells.

[23] By analogy with equation (23), we tried to derive a unique parameterization that would explain the temperature jump ΔT_{TBL} in the top TBL of a mixed heated spherical shell. First, we tested equation (13) against the numerical experiments of Deschamps et al. [2010], and found that it does not explain the temperature jump across the top TBL observed in these experiments. Following the same reasoning as for the average temperature, and noting that for bottom heated shells the temperature jump across the top TBL is well explained by $f^2/(1+f^2)$, we have then tested a parameterization of the form

$$\Delta T_{TBL} = \frac{f^2}{1+f^2} + (d_1 + d_2f) \left[\frac{(1+f+f^2)}{3} \right]^{0.75} \frac{h^{0.75}}{Ra^{0.25}}, \quad (25)$$

where we approximated the Rayleigh number exponent to 1/4 (instead of 0.251). However, nonlinear inversion of mixed heated shells data in Deschamps et al. [2010] could not provide suitable values of d_1 and d_2 . The best fitting solution (blue squares in Figure 9) has a χ^2 around 3000, indicating that it does not explain the input data set. We performed another inversion in which the exponents of Ra and h were allowed to vary, but still could not find any set of parameters explaining all our data set. The best fitting solution (orange squares in Figure 9) has large a χ^2 , around 600. Therefore, according to our calculations and those of Deschamps et al. [2010], the temperature jump across the top TBL cannot be explained by one single parameterization. This result confirms that of Deschamps et al. [2010], which showed that the surface observed heat flux in pure bottom heating and mixed heating experiments cannot be explained by a unique parameterization. It suggests that convection in mixed heated spherical shells cannot be described by mechanisms similar to those observed in volumetrically heated fluids. Again, an obvious difference, compared to volumetric heating fluids, is the presence of hot instabilities rising from the bottom. These instabilities interact with this TBL, thus modifying the removal of the top TBL and the

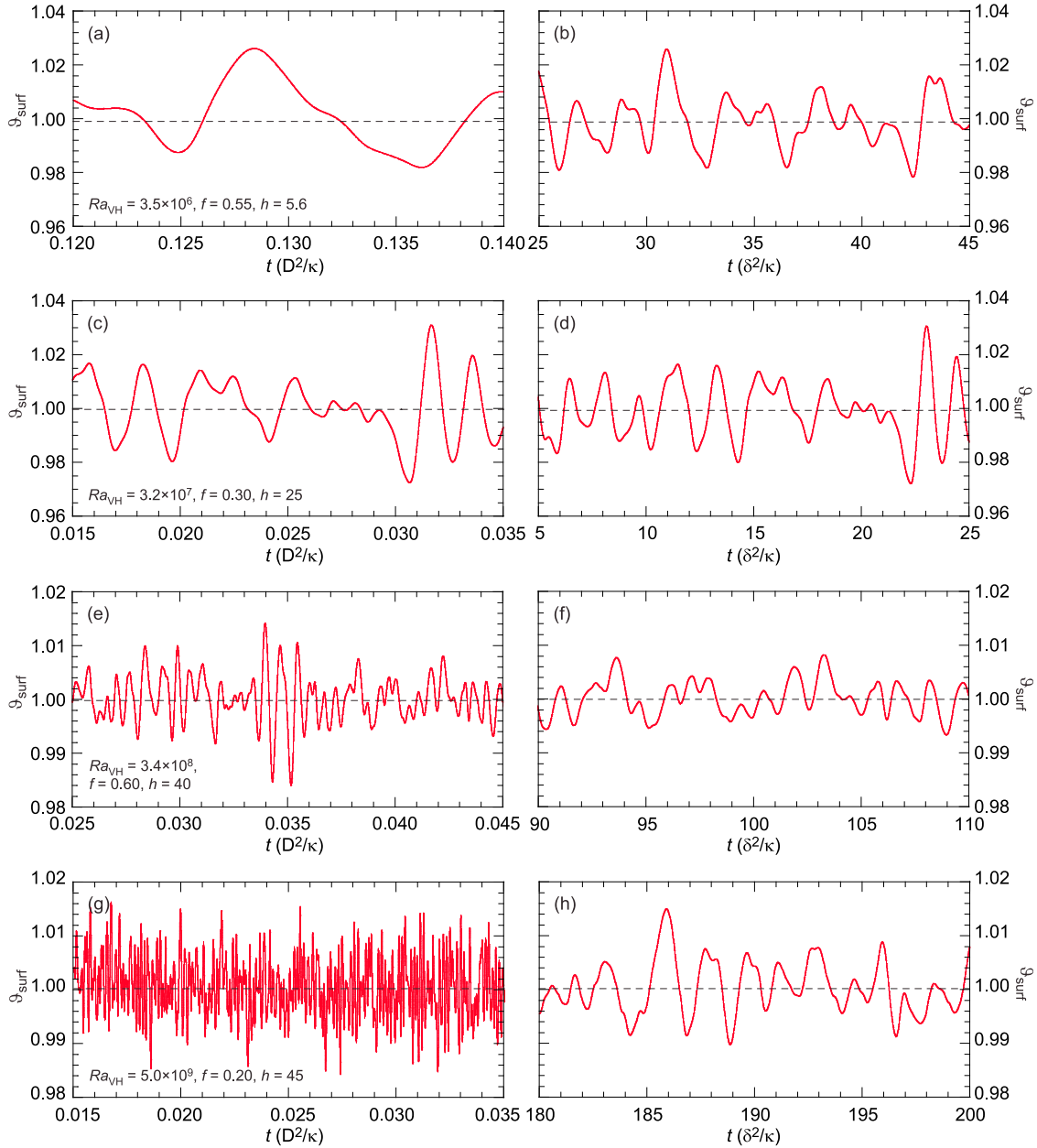


Figure 6. Time-variations of the observed non-dimensional surface heat flux for 4 cases. (left) Time is scaled with the characteristic diffusion time, D^2/κ . (right) Time is scaled with the characteristic time for the growth of instabilities in the TBL t_c , equation (21).

heat transfer through the system [Labrosse, 2002; Moore, 2008].

6. Conclusions and Perspectives

[24] The numerical experiments of thermal convection in a volumetrically heated shell we performed indicate that the scenario proposed by Parmentier and Sotin [2000] to describe isoviscous thermal convection in volumetrically heated Cartesian boxes is also valid in spherical geometry. The cooling of the fluid is controlled by both new instabilities in the thermal boundary layer, and persistent cold plumes

issued from previous instabilities. When quasi-equilibrium is reached, the development of new instabilities is balanced by the merging of cold plumes, and the surface heat flux oscillates around a constant time-averaged value. Regardless of the geometry, 3D-Cartesian boxes with various aspect ratios [Parmentier and Sotin, 2000; this study] or spherical shells with various curvatures (this study), the volume average temperature and the temperature jump across the TBL only depend on the Rayleigh number Ra_{VH} and scale as $Ra_{\text{VH}}^{-0.238}$ and $Ra_{\text{VH}}^{-1/4}$, respectively. The conductive time for growth of instabilities in the TBL is also a power law of Ra_{VH} and scales as $Ra_{\text{VH}}^{-1/2}$.

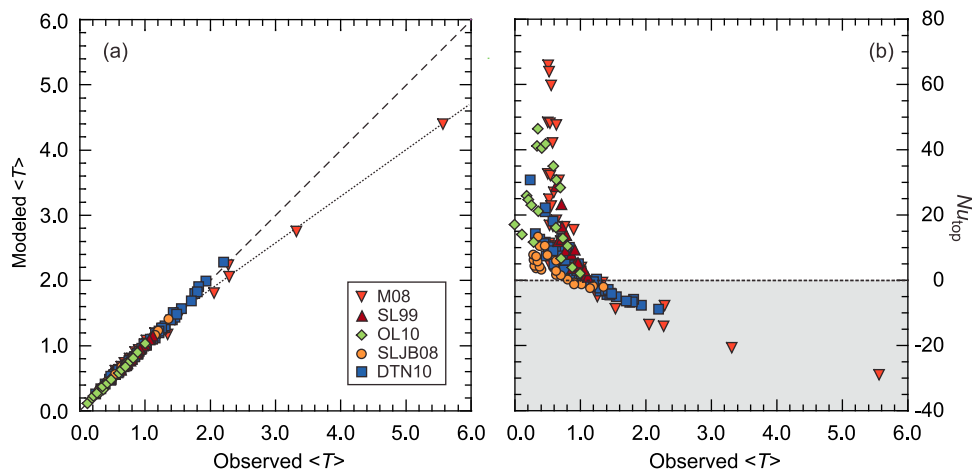


Figure 7. (a) Comparison between observed and modeled average temperatures for convection in mixed heated shells. Modeled temperatures are calculated from equation (23). Light red triangles are from *Moore* [2008], dark red triangles 3D-Cartesian from *Sotin and Labrosse* [1999], green diamonds from *O’Farrell and Lowman* [2010], orange circles from *Shahnas et al.* [2008], and blue squares from *Deschamps et al.* [2010]. (b) Non-dimensional bottom heat flux versus average temperature. The color code for the different data sets is the same as in Figure 7a.

[25] A limitation of our parameterizations is that they were determined for an isoviscous fluid. Planetary materials have a more complex rheology, and in most cases their viscosity strongly depends on temperature. If the thermal viscosity contrast is large enough, a conductive lid is generated at the top of the fluid, and the heat transfer through the fluid is substantially reduced [e.g., *Davaille and Jaupart*, 1993; *Moresi and Solomatov*, 1995; *Deschamps and Sotin*, 2000]. For a volumetrically heated fluid, *Davaille and Jaupart* [1993] have shown that most of the viscosity contrast is accommodated by the conductive lid, and that the fluid layer beneath the lid behaves as an isoviscous fluid. Combined with appropriate corrections accounting for the presence of a stagnant lid at the top of spherical shells [e.g., *Davaille and Jaupart*, 1993; *Grasset and Parmentier*, 1998] our parameterizations may thus be applied to the thermal evolution of icy moons and dwarf planets. In particular, since they are

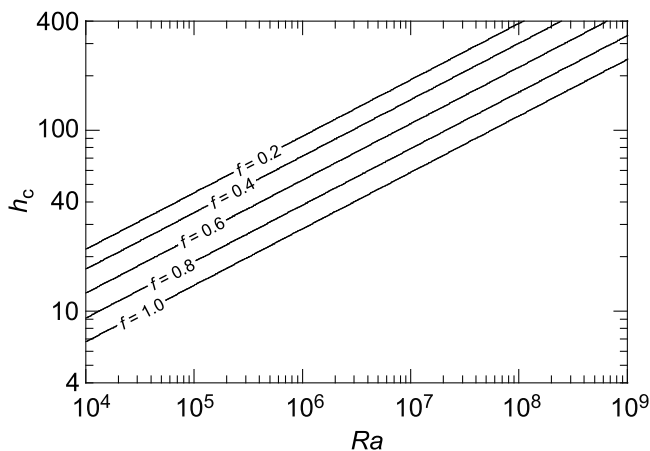


Figure 8. Critical internal heating h_c as a function of Rayleigh number for several values of f . h_c is calculated following equation (23) and assuming that the upper limit for the validity of equation (23) is $T_c = 1.0$.

independent of the geometry, i.e., they do not depend on the value of f , at least for the range of value we explored ($0.2 \leq f \leq 1.0$), the parameterizations derived in this work may be used to estimate thermal properties of planetary cores, provided that these cores have already completed their crystallization and that no intrinsic magnetic field is generated in these bodies.

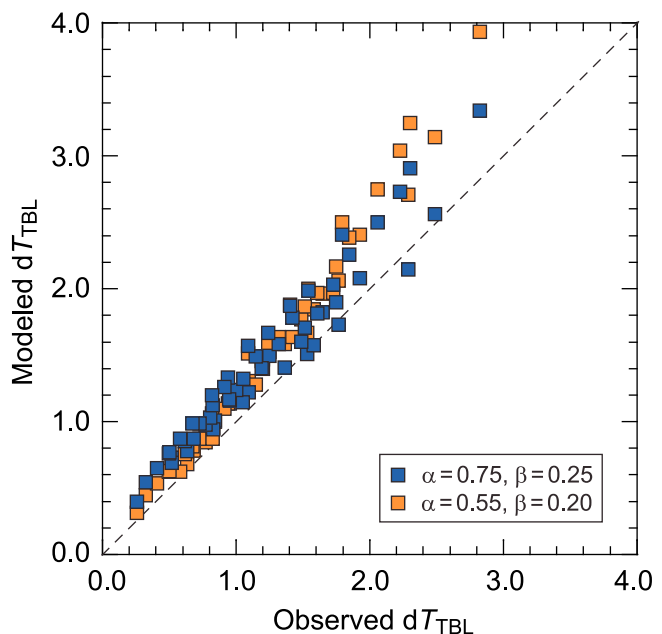


Figure 9. Comparison between observed and modeled temperature jump in the top TBL. Blue squares show the best fit solution to equation (24), where the exponents of Ra and h were fixed to $\alpha = 0.75$ and $\beta = 0.25$, respectively. Orange squares show the best fit solution to a modified version of equation (24), in which the exponents of Ra and h were set as free parameters of the inversion.

[26] **Acknowledgments.** We are grateful to two anonymous colleagues and to the Associate Editors (Mark Wieczorek and Francis Nimmo) for their useful reviews and comments. The research presented in this paper was partly funded by ETH research grant ETHIRA 0-20667-10 and by the National Science Council of Taiwan (NSC grant 101-2116-M-001-001-MY3). All numerical experiments were performed on the ETH's Linux cluster Brutus.

References

- Davaille, A., and C. Jaupart (1993), Transient high-Rayleigh number thermal convection with large viscosity variations, *J. Fluid Mech.*, *253*, 141–166, doi:10.1017/S0022112093001740.
- Deschamps, F., and C. Sotin (2000), Inversion of two-dimensional numerical convection experiments for a fluid with a strongly temperature-dependent viscosity, *Geophys. J. Int.*, *143*, 204–218, doi:10.1046/j.1365-246x.2000.00228.x.
- Deschamps, F., P. J. Tackley, and T. Nakagawa (2010), Temperature and heat flux scalings for isoviscous thermal convection in spherical geometry, *Geophys. J. Int.*, *182*, 137–154.
- Grasset, O., and E. M. Parmentier (1998), Thermal convection in a volumetrically heated, infinite Prandtl number fluid with strongly temperature dependent viscosity: Implication for planetary thermal evolution, *J. Geophys. Res.*, *103*, 18,171–18,181, doi:10.1029/98JB01492.
- Howard, L. N. (1966), Convection at high Rayleigh number, in *Proceedings of the 11th International Congress on Applied Mechanics*, edited by H. Gortler, pp. 1109–1115, Springer, New-York.
- Jarvis, G. T., G. A. Glatzmaier, and V. I. Vangelov (1995), Effect of curvature, aspect ratio, and planform in two- and three-dimensional spherical models of thermal convection, *Geophys. Astrophys. Fluid Dyn.*, *79*, 147–171, doi:10.1080/03091929508228995.
- Kageyama, A., and T. Sato (2004), “Yin-Yang grid”: An overset grid in spherical geometry, *Geochem. Geophys. Geosyst.*, *5*, Q09005, doi:10.1029/2004GC000734.
- Labrosse, S. (2002), Hotspots, mantle plumes, and core heat loss, *Earth Planet. Sci. Lett.*, *199*, 147–156, doi:10.1016/S0012-821X(02)00537-X.
- McNamara, A. K., and S. Zhong (2005), Degree-one mantle convection: Dependence on internal heating and temperature-dependent rheology, *Geophys. Res. Lett.*, *32*, L01301, doi:10.1029/2004GL021082.
- Moore, B. W. (2008), Heat transport in a convecting layer heated from within and below, *J. Geophys. Res.*, *113*, B11407, doi:10.1029/2006JB004778.
- Moresi, L.-N., and V. S. Solomatov (1995), Numerical investigation of 2D-convection with extremely large viscosity variations, *Phys. Fluids*, *7*, 2154–2162, doi:10.1063/1.868465.
- O’Farrell, K. A., and J. P. Lowman (2010), Emulating the thermal structure of spherical shell convection in plane-layer geometry mantle convection models, *Phys. Earth Planet. Inter.*, *182*, 73–84, doi:10.1016/j.pepi.2010.06.010.
- Parmentier, E. M., and C. Sotin (2000), Three-dimensional numerical experiments on thermal convection in a very viscous fluid: Implications for the dynamics of a thermal boundary layer at high Rayleigh number, *Phys. Fluids*, *12*, 609–617, doi:10.1063/1.870267.
- Schubert, G., D. L. Turcotte, and P. Olson (2001), *Mantle Convection in the Earth and Planets*, 940 pp., Cambridge Univ. Press, XX, doi:10.1017/CBO9780511612879.
- Shahnas, M. H., J. P. Lowman, G. T. Jarvis, and H.-P. Bunge (2008), Convection in a spherical shell heated by an isothermal core and internal sources: Implication for the thermal state of planetary mantles, *Phys. Earth Planet. Inter.*, *168*, 6–15, doi:10.1016/j.pepi.2008.04.007.
- Smolarkiewicz, P. K. (1984), A fully multidimensional positive definite advection transport algorithm with small implicit diffusion, *J. Comput. Phys.*, *54*, 325–362, doi:10.1016/0021-9991(84)90121-9.
- Sotin, C., and S. Labrosse (1999), Three-dimensional thermal convection in an iso-viscous, infinite Prandtl number fluid heated from within and from below: Application to the transfer of heat through planetary mantles, *Phys. Earth Planet. Inter.*, *112*, 171–190, doi:10.1016/S0031-9201(99)00004-7.
- Stüben, K., and U. Trottenberg (1982), Multigrids methods: Fundamental algorithms, model problem analysis and applications, in *Multigrids Methods*, edited by W. Hackbusch and U. Trottenberg, pp. 1–175, Springer, Berlin.
- Tackley, P. J. (2008), Modelling compressible mantle convection with large viscosity contrasts in a three-dimensional spherical shell using the yin-yang grid, *Phys. Earth Planet. Inter.*, *171*, 7–18, doi:10.1016/j.pepi.2008.08.005.
- Tarantola, A., and B. Valette (1982), Generalized nonlinear inverse problems solved using the least square criterion, *Rev. Geophys.*, *20*, 219–232, doi:10.1029/RG020i002p00219.
- Tobie, G., A. Mocquet, and C. Sotin (2005), Tidal dissipation within large icy satellites: Applications to Europa and Titan, *Icarus*, *177*, 534–549, doi:10.1016/j.icarus.2005.04.006.
- Travis, B., and P. Olson (1994), Convection with internal sources and turbulence in the Earth’s mantle, *Geophys. J. Int.*, *118*, 1–19, doi:10.1111/j.1365-246X.1994.tb04671.x.
- Vangelov, V. I., and G. T. Jarvis (1994), Geometrical effects of curvature in axisymmetric spherical models of mantle convection, *J. Geophys. Res.*, *99*, 9345–9358, doi:10.1029/93JB03133.
- Zebib, A., G. Schubert, J. L. Dein, and R. C. Paliwal (1983), Character and stability of axisymmetric thermal convection in spheres and spherical shells, *Geophys. Astrophys. Fluid Dyn.*, *23*, 1–42, doi:10.1080/03091928308209038.